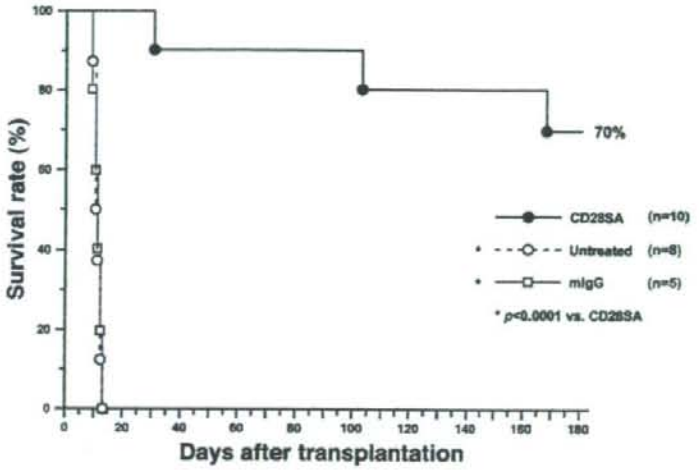

Figure 1: Survival of recipients treated with CD28 SA. The Kaplan–Meier curve of graft survival demonstrates that CD28 SA (closed circle) significantly prolonged graft survival until more than 180 days of follow-up ($p < 0.05$ vs. untreated group and mIgG group), while no animals survived more than 14 days in the untreated group (open circle) or the mIgG group (open square).

Flow cytometric analysis

The spleen, kidney allograft and peripheral blood were recovered from recipients subjected to each treatment. Single-cell suspensions were prepared and mixed with 10 μg/mL of allophycocyanin (APC)-conjugated anti-CD4 and phycoerythrin (PE)-conjugated anti-CD25 (BD Pharmingen, San Jose, CA) for 30 min. For the FOXP3 staining, cells were fixed and permeabilized for 3 h and stained with fluorescein isothiocyanate (FITC)-anti-FOXP3 according to manufacturer's instructions (eBiosciences). Cells were analyzed by multiparameter flow cytometry using FACScan (BD Biosciences) and data analysis was performed using FlowJo software (Treestar, Ashland, OR). The percentages of CD4-positive cells and CD25– and FOXP3-expressing cells among CD4-positive cells from three animals per group were averaged.

Adoptive transfer of CD4+CD25+ cells in the acute rejection model

The spleen from a Lewis rat was recovered 3 days after the injection of CD28 SA and CD4+CD25+ cells or CD4+CD25– cells were extracted from it using the magnetic beads technique. We performed adoptive transfer by triple injection of a cell suspension [1×10^7 CD4+CD25+ cells (CD25+ group) or CD4+CD25– cells (CD25– group) in 0.5 mL of saline] into the Lewis recipients 3 days before, on the day of and 3 days after engraftment of the kidney from the Wistar rats. The recipients in the CD25+ group, surviving for 120 days, received bilateral cardiac allografts from both donor-matched Wistar and third-party BN in each animal on day 120 (12).

Results

CD28 SA significantly prolongs graft survival

We first examined the therapeutic effect of CD28 SA on renal transplantation by evaluating graft survival in our established acute graft rejection model (11). As we reported previously (11), all disease control recipients left either untreated (untreated group) or treated with mouse IgG (mIgG group), died by day 13 due to renal failure (untreated group: median 10 days; range 9–13 days; 1st–3rd quarter [Qu] = 10–12 days; mIgG group: median 11 days; range 9–13 days; 1st–3rd Qu = 10–12 days; Figure 1). In contrast, 90% of CD28 SA-treated recipients (CD28 SA group) survived for over 100 days, and seven recipients (70%) survived in an apparently healthy state until the day of graft recovery at 180 days (median infinity (INF); range 30 to INF; 1st–3rd Qu = 168 to INF days).

CD28 SA significantly protects graft function

Graft function was assessed serially by measuring urine volume and serum creatinine levels, and urinary sediment was examined in each sample. Functional data clearly validated the data for graft survival and confirmed the beneficial effects of CD28 SA on renal transplantation. The disease control recipients from the untreated group showed marked hematuria by day 2 after transplantation. The urine volume was decreased significantly on day 6 compared with that on day 2 (1.86 ± 1.30 mL/day and 11.16 ± 6.20 mL/day, respectively, $n = 8$, $p < 0.05$,), and most animals became anuric by day 10 (0.35 ± 0.70 mL/day, $n = 4$) (Figure 2A). In contrast to the disease control, all recipients in the CD28 SA group maintained a normal urine volume without hematuria in the acute phase (urine volume; 11.23 ± 3.39 mL/day on day 6, $n = 8$, $p < 0.01$ vs. untreated group) and retained a normal urine volume until the day of graft recovery (9.12 ± 0.89 mL/day on day 180, $n = 6$), which was equivalent to that in the age-matched isograft group (8.16 ± 2.08 mL/day, $n = 5$, $p = 0.37$ vs. CD28 SA group; Figure 2A).

The serum creatinine data clearly corroborated the data for urine volume. In the untreated group, the levels of serum creatinine increased by day 6 (3.02 ± 1.48 mg/dL, $n = 8$) and increased progressively thereafter until death (5.03 ± 0.71 mg/dL on day 10, $n = 5$). In contrast, the serum creatinine levels were significantly lower at all time points in recipients from the CD28 SA group in the acute phase (0.84 ± 0.36 mg/dL on day 6, $n = 10$ vs. untreated

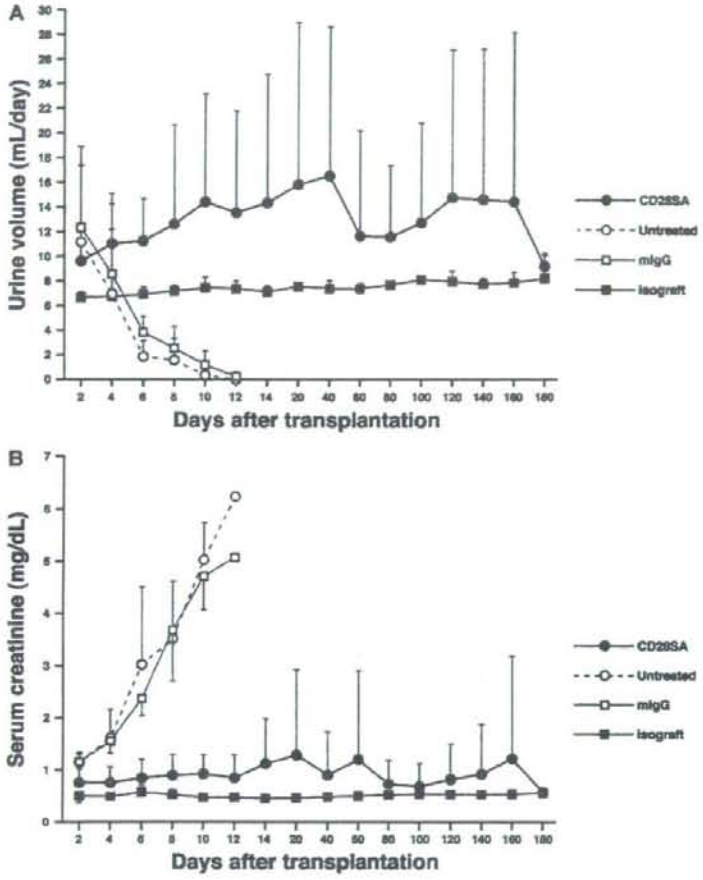

Figure 2: Graft function of recipients treated with CD28 SA. Graft function was analyzed by serial measurement of urinary volume (A) and serum creatinine (B).

group, $p < 0.01$, Figure 2B), and these recipients retained normal renal function with creatinine levels similar to those of age-matched isograft controls until the day of graft recovery at 180 days [0.57 ± 0.08 mg/dL ($n = 6$) and 0.56 ± 0.06 mg/dL ($n = 5$) in CD28 SA group and isograft group, respectively; $p = 0.86$, Figure 2B].

CD28 SA significantly preserves graft histology

Consistent with the functional data, histological examination also confirmed the beneficial effects of CD28 SA. Disease control allografts from the mIgG group and the untreated group recovered on day 6 after transplantation showed florid infiltration of mononuclear cells with hemorrhage and marked disruption of the normal renal architecture. Many tubules showed severe tubulitis with marked structural deformity or necrosis with protein deposition and intratubular casts (Figure 3A). Many glomeruli showed numerous infiltrating mononuclear cells with mesangial matrix expansion (Figure 3B). Arteries showed transmural arteritis with arterial fibrinoid change and necrosis of medial smooth muscle cells with accompanying lymphocytic inflammation (Figure 3C). In contrast to disease control recipients, CD28 SA markedly preserved the structure of the allograft throughout the graft tissue, despite considerable mononuclear cell infiltration (Figure 3D). No glomeruli showed mesangial matrix expansion (Figure 3E). Arteries mostly retained a normal structure, without intimal proliferation, fibrinoid change or necrosis (Figure 3F). Assessment of tubulointerstitial damage by immunohistochemical detection of vimentin, a marker of tubulointerstitial damage, which is associated with phenotypic transformation of cells (13), showed increased staining in the tubular cells of the mIgG-treated allograft (Figure 3G). In contrast, treatment with CD28 SA reduced the degree of tubular cell staining for vimentin (Figure 3H), suggesting that CD28 SA treatment protected tubular cells against acute rejection.

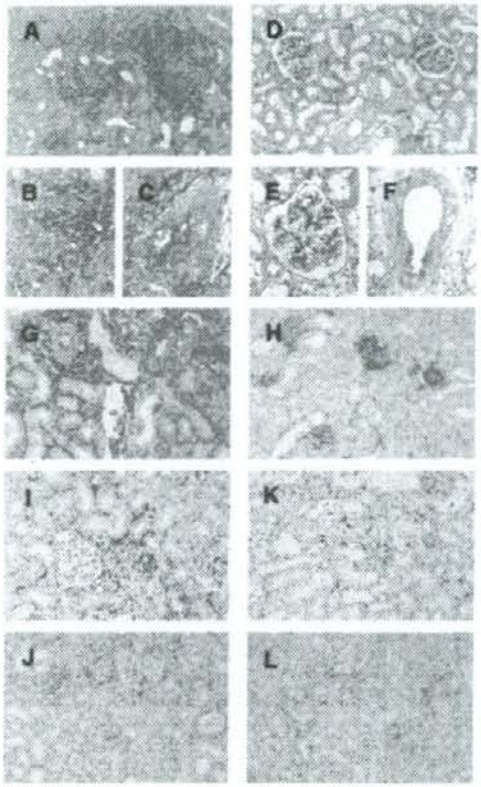

Figure 3: Graft histology after treatment with CD28 SA. Representative photomicrographs of allografts from recipients treated with Cont-IgG (left panels: A–C, G, I, J) or CD28 SA (right panels: D–F, H, K, L) and stained for PAS (A–F), vimentin (G, H), ED-1 (I, K) and FOXP3 (J, L). Original magnification, ×200 in A, D, G–L and ×400 in B, C, E, F.

CD28 SA induces infiltration of Treg cells in allografts

An interesting observation in the present study was considerable infiltration of mononuclear cells into allografts, with significant preservation of the histological structure by CD28 SA. Therefore, we undertook a detailed immunohistological evaluation of allografts from the mIgG group and the CD28 SA group. In the mIgG group, we observed dense and diffuse interstitial infiltration of ED-1-positive macrophages (164 ± 29 cells, Figure 3I), whereas FOXP3-positive Treg cells were scarcely evident (3.1 ± 0.8 cells, $p < 0.0001$ vs. mIgG group; Figure 3J). In contrast, considerable numbers of infiltrating mononuclear cells in the CD28 SA group were not ED-1-positive macrophages (25 ± 12 cells, Figure 3K), but predominantly FOXP3-positive Treg cells (85.3 ± 12.7 cells, $p < 0.001$ vs. mIgG group; Figure 3L). The mechanism whereby CD28 SA inhibits macrophage infiltration but induces Treg cells remains unclear. It may be an indirect effect of CD28 SA resulting from suppression of acute rejection. The expanded Treg cells protected tubulointerstitium from acute rejection, and consequently the decreased tubulointerstitial injury suppressed macrophage infiltration. Alternatively, however, CD28 SA-induced Treg cells may directly suppress the macrophage infiltration.

CD28 SA induces Treg cell expansion in recipients

Flow cytometric analysis demonstrated that administration of CD28 SA induced a marked increase in the frequency of CD4-positive cells in peripheral blood, spleen and allograft on day 6 after transplantation, [65.2 ± 4.2% ($p < 0.05$ vs. naïve Lewis rats), 46.9 ± 2.8% ($p < 0.05$ vs. naïve Lewis rats) and 10.3 ± 1.6% ($p < 0.01$ vs. naïve Lewis rats), respectively] as compared with naïve Lewis rats (45.9 ± 5.3%, 18.9 ± 1.7%, and 0.3 ± 0.1%, Figure 4A). As treatment with CD28 SA enlarges the size of the spleen and lymph nodes (2.9- to 3.2-fold) along with expansion of T cells (3.1- to 3.5-fold), the absolute number of CD4-positive cells was expected to increase more dramatically. In addition, CD28 SA treatment led to an increase in the frequency of CD25-expressing cells among CD4-positive cells in peripheral blood, spleen and allograft relative to treatment with triple intravenous injection of mouse IgG (mIgG group) or untreated naïve Lewis rats [31.8 ± 4.1% ($p < 0.05$ vs. mIgG group and naïve Lewis rats), 16.3 ± 2.2% ($p < 0.05$ vs. mIgG group and naïve Lewis rats) and 29.8 ± 3.4% ($p < 0.05$ vs. mIgG group and naïve Lewis rats) in the CD28 SA group, 5.0 ± 1.6%, 7.3 ± 1.9% and 8.0 ± 2.1% in the mIgG group, 15.7 ± 3.0%, 5.9 ± 1.8% and 18.7 ± 2.4% in naïve Lewis rats, respectively; Figure 4B]. Furthermore, CD28 SA treatment increased FOXP3-positive Treg cells in peripheral blood, spleen and allograft in comparison with mIgG-treated disease controls or untreated naïve Lewis rats [55.3 ± 7.7% ($p < 0.01$ vs. mIgG group and naïve Lewis rats), 38.6 ± 9.2% ($p < 0.05$ vs. mIgG group and naïve Lewis rats) and 71.1 ± 10.4% ($p < 0.001$ vs. mIgG group and naïve Lewis rats) in the CD28 SA group, 8.9 ± 1.0%, 12.9 ± 1.6% and 15.9 ± 2.7% in the mIgG group, 9.4 ± 1.5%, 12.4 ± 2.1% and 15.3 ± 2.0% in naïve Lewis rats, respectively; Figure 4C]. It is of interest that CD28 SA treatment especially increased the infiltration of Treg cells into allografts in comparison with the peripheral blood and spleen.

Treatment with CD28 SA induces donor-specific tolerance

To examine whether CD28 SA can induce donor-specific tolerance or nonspecific immunosuppression, all CD28 SA-treated recipients, which accepted allograft kidney for 120 days ($n = 7$), received bilateral cardiac allografts from both donor-matched Wistar and third-party BN in each animal on day 120. Age-matched first cardiac allograft model rats (Wistar to naïve Lewis; control group) were used as

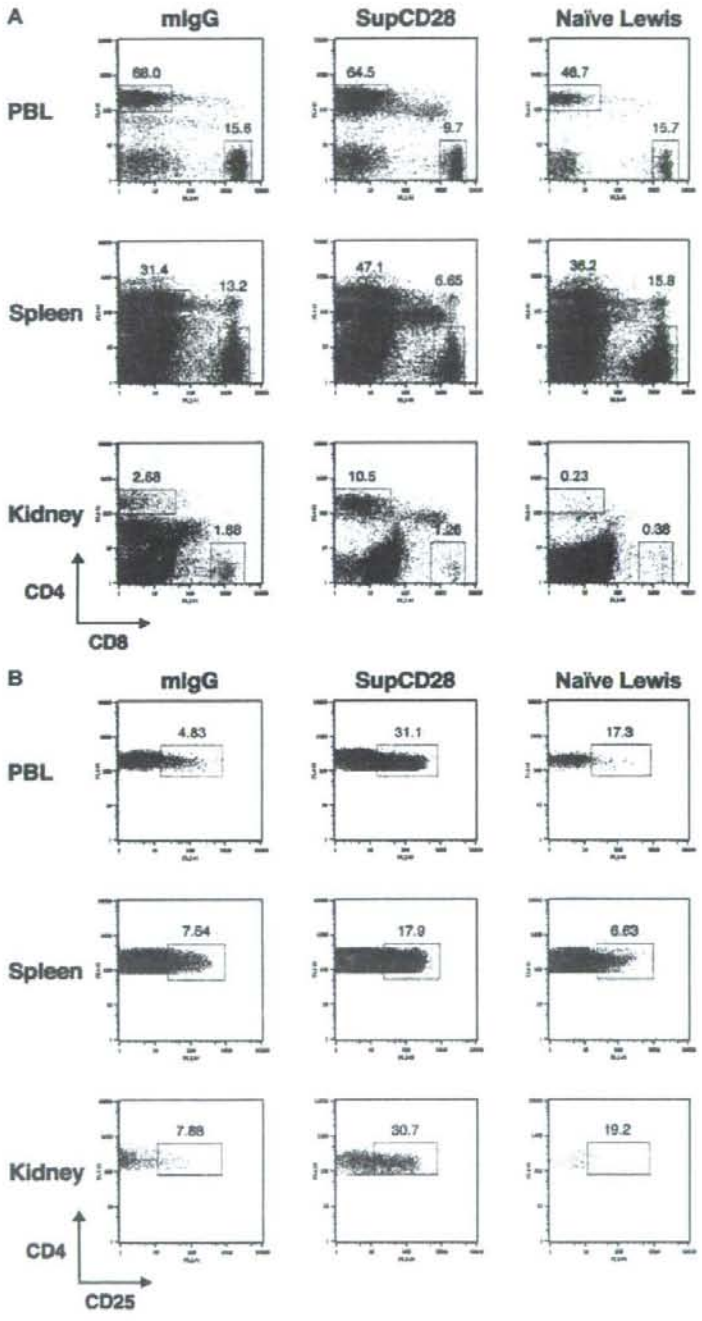

Figure 4: Increase of regulatory T cells in treated recipients. Representative flow cytometric analysis of CD4+/CD8+ (A), CD4+CD25+ (B) and CD4+FOXP3+ (C) expression on the cells extracted from peripheral blood, spleen or allografts of recipients treated with mIgG or CD28 SA or naïve Lewis rats, respectively. The numbers in each panel represent the percentage of CD4+ and CD8+ lymphocytes (A), CD25-positive (B) or FOXP3-positive (C) population in CD4+ T cells. CD28 SA significantly expanded CD4+CD25+ and CD4+FOXP3+ Treg cells in renal allografts as well as in peripheral blood and spleen.

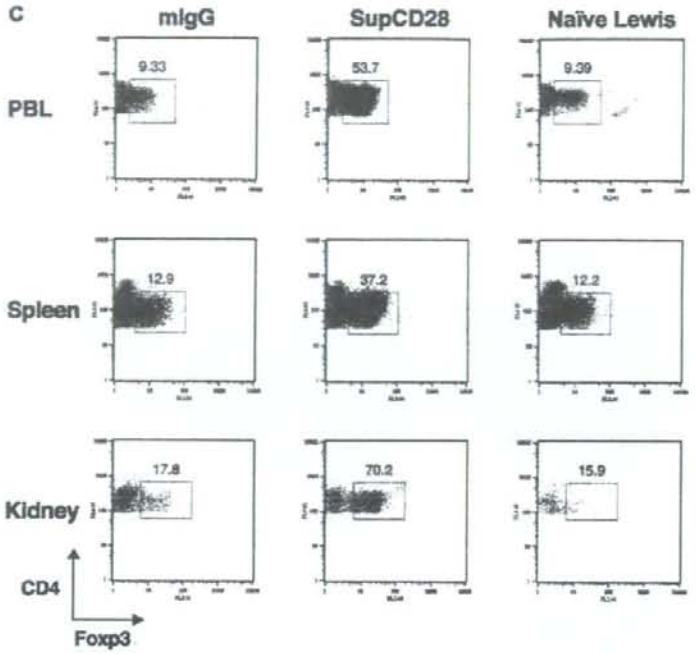

Figure 4: Continued.

controls in the rat cardiac allograft model (n = 5). Interestingly, six recipients (85.7%) exhibited donor-specific acceptance, as they accepted donor-matched Wistar heart grafts without application of any immunosuppressive drugs or additional CD28 SA treatment; these animals survived with normally beating Wistar cardiac allografts until the day of recovery on day 180, but they acutely rejected third-party BN grafts (median survival period 9 days, range 8–10 days; 1st–3rd Qu = 8–9 days; Figure 5A), while age-matched control Lewis rats rejected Wistar heart grafts within 10 days (median survival period 8 days, range 7–10 days; 1st–3rd Qu = 8–9 days). Representative hematoxylin and eosin (HE) sections from donor-matched Wistar cardiac allografts (Figure 5B) and third-party BN cardiac allografts (Figure 5C) recovered on day 6 showed classical signs of acute rejection, including strong interstitial infiltration of mononuclear cells with severe hemorrhage, edema and necrosis in third-party BN cardiac allografts, but a normal graft histology with no such signs of acute rejection in Wistar cardiac allografts.

Treatment with CD28 SA preserves long-term graft structure

We examined the kidney allografts from CD28 SA-treated donor-specific 'tolerant' recipients 180 days after transplantation by staining with PAS (Figure 6A) and Mallory Azan (Figure 6B) and also immunohistochemically for αSMA (Figure 6C) and vimentin (Figure 6D). This revealed only faint fibrosis; most glomeruli showed a sparse mesangial matrix with no thickening of the basement membrane, and most arteries retained a normal appearance. Staining for vimentin demonstrated no tubule injury (Figure 6D).

Adoptive transfer of CD4+CD25+ cells induces donor-specific tolerance

In order to examine whether the CD28 SA-induced tolerance was caused directly by CD28 SA or indirectly by CD28 SA-expanded CD4+CD25+ Treg cells, we performed adoptive transfer experiments with CD4+CD25+ or CD4+CD25− cells, which had been purified from naïve Lewis rats injected with CD28 SA. All six recipients treated with adoptive transfer of CD4+CD25− cells (CD25− group) rejected renal allograft and died by day 13 (median 11 days; range 9–13 1st–3rd Qu = 10.3–11.8 days). In contrast, all six recipients treated with adoptive transfer of CD4+CD25+ cells (CD25+ group) survived for more than 25 days after the transplantation and two of them survived until day 180 (CD25+ group; median 77 days, range 26 to INF; 1st–3rd Qu = 34.8 to INF days; $p = 0.0006$ vs. CD25− group; Figure 7). We also performed secondary cardiac bilaterally allografting using both donor-matched Wistar heart and third-party BN heart simultaneously on day 120 after transplantation in two of the long-surviving adoptive transfer recipients of CD4+CD25+ cells. The adoptive transfer recipients also exhibited donor-specific acceptance, accepting donor-matched and

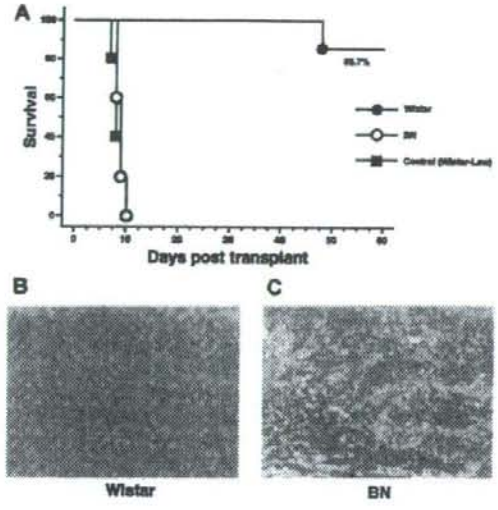

Figure 5: Donor-specific tolerance after treatment with CD28 SA. The Kaplan–Meier curve (A) of secondary cardiac bi-allografts of both heterotopic Wistar heart (closed circle) and third-party BN heart (open circle) grafted simultaneously on day 120, in order to examine whether CD28 SA can induce tolerance in a donor-specific or nonspecific manner. Age-matched naïve Lewis rats received Wistar heart as a control cardiac allograft model (open square). Representative histological features of transplanted Wistar heart (B) and BN heart (C) were examined by HE staining. Original magnification ×100.

normally beating Wistar cardiac grafts until the day of recovery on day 180, but acutely rejecting third-party BN grafts by day 9. In addition, histological examination revealed that the kidney allografts recovered on day 180 had excellent tissue preservation, despite considerable mononuclear cell infiltration. Most glomeruli and tubuli remained normal with no apparent mesangial matrix or protein deposition.

Discussion

In this study, we demonstrated that treatment with CD28 SA can induce donor-specific tolerance of MHC-incompatible rat renal allografts in inbred strains. This is the first study to assess the role of a superagonistic antibody in a renal transplant model. Moreover, the superagonistic CD28 SA seems superior to conventional anti-CD28 antibodies, which are unable to induce indefinite graft survival and tolerance despite prolonged graft survival in an acute rejection model (5). The following key findings support this conclusion: (1) Injection of CD28 SA expanded CD4+CD25+FOXP3+ Treg cells in transplanted allografts as well as in peripheral blood and spleen. (2) In an acute rejection model, treatment with CD28 SA significantly prolonged animal survival (>120–180 days) with good preservation of graft function and histological structure, and these long-surviving recipients exhibited donor-specific tolerance, accepting donor-matched Wistar, but acutely rejecting third-party BN, cardiac allografts. (3) Adoptive transfer of polyclonal CD4+CD25+ cells, recovered from CD28 SA-treated naïve Lewis rats, also succeeded in inducing donor-specific tolerance. These observations suggest that CD28 SA-induced expanded CD4+CD25+FOXP3+ Treg cells are able to induce donor-specific tolerance.

The ultimate goal of organ transplantation is to establish graft tolerance whereby recipients do not require continuous administration of systemically immunosuppressive drugs. Natural CD4+CD25+ Treg cells have several immunological features, which are important for their use in inducing or attenuating immunological tolerance to self or nonself antigens. The TCR repertoire of natural CD4+CD25+ Treg cells is as broad and diverse as that of CD4+CD25− T cells but is skewed more than the latter toward recognizing complexes of self peptide and MHC expressed in the thymus and periphery (14,15). They can recognize allogeneic transplantation antigens (16) and therefore when stimulated can suppress graft rejection.

Graca et al. showed that alloantigen-specific Treg cell activity has been detected in naïve, unmanipulated recipients in a skin-graft model; however, a minimum of 10-fold more CD4+CD25+ T cells was required for graft acceptance (17). Hunig et al. reported that functional Treg cells are preferentially expanded *in vivo*, leading to a 20-fold increase within 3 days in response to a single administration of CD28 SA (8). Hence, our observation suggests that sufficient allospecific Treg cells could expand and infiltrate into the allograft to protect it against the alloreactive effector T cells. In this context, it was recently shown in a mouse system that *in vivo* treatment with mouse CD28 SA activates and expands both CD103-negative and CD103-positive subsets of CD4+CD25+ Treg cells (18). The latter population is known to home to inflamed tissues and to act locally to suppress immune responses (19).

Immunotherapy with conventional anti-CD28 antibodies was previously shown to work through mechanisms including receptor internalization (5), TCR-ClassII-B7+ regulatory cells (20) and induction of antigen-specific T-cell death (21). However, indefinite graft survival and tolerance could not be induced by conventional anti-CD28 antibody treatment (5). On the other hand, the most important finding of our study is that superagonistic CD28 SA expanded CD4+CD25+FOXP3+ Treg cells and induced graft-specific tolerance. One possible way of using natural CD4+CD25+ Treg cells to induce graft-specific tolerance without hampering immune responses to allograft antigens is to prepare an immunological condition facilitating antigen-specific spontaneous population expansion of natural Treg cells by controlling graft-reactive effector

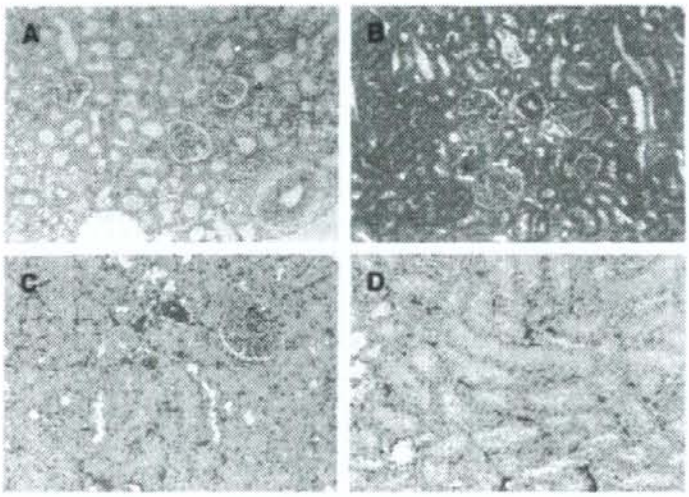

Figure 6: Histology of grafts from long-surviving recipients treated with CD28 SA. Representative photomicrographs of allografts from recipients treated with CD28 SA recovered 180 days after transplantation stained with PAS (A), Mallory Azan (B) and immunohistochemically for αSMA (C) and vimentin (D). Original magnification ×200.

T cells. Although treatment with CD28 SA expanded the CD4+CD25+FOXP3+ Treg cells, these natural Treg cells are considered to be suppressive in an antigen-nonspecific manner before antigen exposure. It is highly likely, however, that allogeneic MHC stimulation can expand antigen-specific Treg cells through the indirect pathway (22,23). In addition, a dynamic balance must be attained and maintained between allospecific Treg cells and alloreactive effector T cells in 'tolerant' animals, the former continuously and actively suppressing the latter. Furthermore, only allospecific Treg cells are likely to expand during sustained exposure to the allograft. Supporting this notion, CD28 SA-treated long-surviving recipients exhibited donor-specific tolerance, accepting donor-matched Wistar, but acutely rejecting third-party BN, cardiac allografts 120 days after transplantation without further treatment.

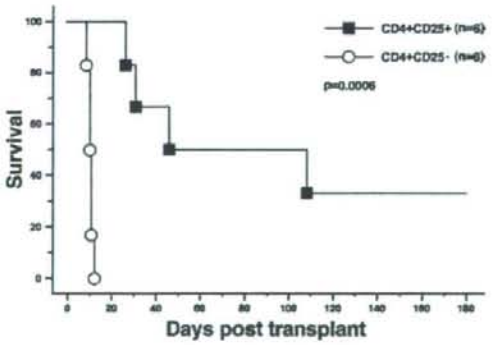

Figure 7: Survival of recipients treated with adoptive transfer of CD4+CD25+ cells. The Kaplan–Meier curve of graft survival demonstrated that adoptive transfer of CD4+CD25+ cells (closed circle) significantly prolonged graft survival compared with adoptive transfer of CD4+CD25− cells (open circle; p = 0.0006).

In order to test if the induction of tolerance in this acute rejection model was indeed mediated by CD28 SA-expanded CD4+CD25+ Treg cells, we performed adoptive transfer experiments with CD4+CD25+ cells, which were purified by *in vivo* injection of CD28 SA. Naïve Lewis rats were primed with CD28 SA 3 days before isolation of CD4+CD25+ and CD4+CD25− T cells from the spleen. All six recipients treated with adoptive transfer of CD4+CD25+ T cells showed significantly prolonged survival, while CD4+CD25− conventional T cells purified from the same rats were not therapeutic in this model. More importantly, two of these long-surviving recipients accepted secondary Wistar cardiac allografts, but rejected third-party BN allografts, indicating that the adoptive transfer of antigen-nonspecific Treg cells was also able to develop donor-specific tolerance. Thus, nonantigen-specific CD4+CD25+ Treg cells, purified from CD28 SA-treated naïve rats successfully induced donor-specific tolerance in this acute rejection model. The next goal should be to increase the tolerance induction rate, as in the present study this was less than 40%. In this experiment, we were unable to employ CD4+CD25+ cells purified from untreated naïve Lewis rats as a control adoptive transfer, because a sufficient number of CD4+CD25+ cells could not be isolated. It is not clear whether the therapeutic effects of CD4+CD25+ cells purified from CD28 SA-treated rats depend solely on the number of expanded Treg cells or whether CD4+CD25+ cells acquire a specific property that allows them to suppress acute rejection. Further experiments will be needed to clarify whether CD4+CD25+

cells purified from CD28 SA-treated rats have a therapeutic effect superior to that of cells extracted from untreated naïve rats.

Recently, in a Phase I trial of the anti-CD28 monoclonal antibody TGN 1412 (human-antibody counterpart of CD28 SA), six healthy male volunteers showed a systemic inflammatory response characterized by rapid induction of proinflammatory cytokines and accompanied by erythema, vasodilation and hypotension (24). This type of cytokine release had not been observed in preclinical studies of TGN 1412 (6,7), and it is currently unclear whether the severe effects of this type of cytokine release *in vivo* in humans are caused by direct ligation of CD28 on T cells or by interaction with cell types not included in the preclinical *in vitro* assays (24,25), resulting in cytokine release *in vitro* if endothelial cells are included. A common feature after infusion of extremely low dose of TGN 1412 was reported to be early acute renal impairment, producing urinary sediment. In our experiments using the acute rejection model, however, treatment with CD28 SA maintained normal urine volume without hematuria and protected the kidneys against functional impairment, consistent with the preclinical trials; the stimulation provided by superagonistic CD28 antibody preferentially activated and expanded CD4+CD25+ Treg cells, resulting in transient lymphocytosis with no detectable toxic or proinflammatory effects (6,7). Although the application of very low dosages of CD28 SA to normal Lewis rats is sufficient to induce Treg cell expansion *in vivo* without the generalized lymphocytosis observed with high doses of CD28 SA (6), CD28 SA at 0.5 mg induced lymphocytosis, but did not induce renal injury in our study. Our observation suggests that a systemic inflammatory response observed in a Phase I trial of TGN 1412 was likely independent of lymphocytosis. Although it remains unclear why application of superagonistic CD28 antibody led to a difference in outcome between this Phase I trial (24) and the preclinical trials (6,7), it is suggested that our observations may not be directly applicable in a clinical setting.

The identification of naturally occurring Treg cells with the capacity to suppress allograft rejection suggests that therapies designed to activate and expand this subset could work extremely efficiently in renal transplantation. The development of Treg cells could be promoted *in vivo* by administration of an 'improved CD28 SA', which would also protect the transplant organ from rejection without unexpected side effects. Alternatively, Treg cells could be generated and expanded *in vitro* by manipulating T cells isolated from the recipient. Once characterized, these Treg cells could be re-infused into the transplant recipient. As retransferred Treg cells probably survive in the recipient for long periods of time, one advantage of adoptive transfer of Treg cells might be the induction of long-term peripheral tolerance. Another advantage might be the generation of Treg cells with specificity for the relevant antigen, allowing antigen-specific therapy (26,27). Determining the origin of Treg cells that are involved in the induction and/or maintenance of transplantation tolerance will facilitate the fruition of this strategy. Lin and Hnig showed that Treg cells are preferentially expanded *in vitro* by CD28 SA without the need for TCR engagement (8). Up to 5 $\times 10^8$-fold expansion of rat Treg cells was possible, and the cells were stable in culture for more than 100 days (28). Importantly, the expansion of rat Treg cells was superior to that of conventional T cells (28). Given that Treg cells can be isolated from the recipient in advance and expanded to sufficient numbers by *in vitro* culture with CD28 SA, adoptive transfer of Treg cells generated in this way may be a more efficient approach for increasing the induction rate of donor-specific tolerance in recipients.

In conclusion, we have demonstrated that treatment with CD28 SA can induce donor-specific tolerance in an acute rejection model, probably due to an increase in the alloantigen-specific population of CD4+CD25+ Treg cells. With the possibility of clinical application in mind, it will be necessary to work toward a safe therapy using CD28 SA that avoids the unexpected side effects encountered during the TGN 1412 trial. In addition, further studies should explore whether *in vivo* administration of improved CD28 SA or adoptive transfer of *in vitro*-expanded Treg cells by CD28 SA could be more advantageous and safe for therapeutic application aimed at the induction of tolerance.

Acknowledgment

This work was supported by Wilhelm Sander Stiftung, Deutsche Forschungsgemeinschaft through SFB 479 for TH.

References

1. Sakaguchi S. Naturally arising Foxp3-expressing CD25+CD4+ regulatory T cells in immunological tolerance to self and nonself. Nat Immunol 2005; 6: 345–352.
2. Schwartz RH. Costimulation of T lymphocytes: The role of CD28, CTLA-4, and B7/BB1 in interleukin-2 production and immunotherapy. Cell 1992; 71: 1065–1068.
3. Linsley PS, Ledbetter JA. The role of the CD28 receptor during T cell responses to antigen. Ann Rev Immunol 1993; 11: 191–212.
4. Tacke M, Hanke G, Hanke T, Hunig T. CD28-mediated induction of proliferation in resting T cells *in vitro* and *in vivo* without engagement of the T cell receptor: Evidence for functionally distinct forms of CD28. Eur J Immunol 1997; 27: 239–247.
5. Dengler TJ, Szabo G, Sido B et al. Prolonged allograft survival but no tolerance induction by modulating CD28 antibody JJ319 after high-responder rat heart transplantation. Transplantation 1999; 67: 392–398.
6. Beyersdorf N, Gaupp S, Balbach K et al. Selective targeting of regulatory T cells with CD28 superagonists allows effective therapy of experimental autoimmune encephalomyelitis. J Exp Med 2005; 202: 445–455.
7. Luhder F, Huang Y, Dennehy KM et al. Topological requirements and signaling properties of T cell-activating, anti-CD28 antibody superagonists. J Exp Med 2003; 197: 955–966.

8. Lin CH, Hunig T. Efficient expansion of regulatory T cells *in vitro* and *in vivo* with a CD28 superagonist. Eur J Immunol 2003; 33: 626–638.
9. Evans EJ, Esnouf RM, Manso-Sancho R et al. Crystal structure of a soluble CD28-Fab complex. Nat Immunol 2005; 6: 271–279.
10. Margulies DH. CD28, costimulator or agonist receptor? J Exp Med 2003; 197: 949–953.
11. Azuma H, Tomita N, Kaneda Y et al. Transfection of NFkappaB-decoy oligodeoxynucleotides using efficient ultrasound-mediated gene transfer into donor kidneys prolonged survival of rat renal allografts. Gene Ther 2003; 10: 415–425.
12. Lin H, Bolling SF, Linsley PS et al. Long-term acceptance of major histocompatibility complex mismatched cardiac allografts induced by CTLA4Ig plus donor-specific transfusion. J Exp Med 1993; 178: 1801–1806.
13. Eddy AA. Interstitial nephritis induced by protein overload proteinuria. Am J Pathol 1989; 135: 719–733.
14. Hsieh CS, Liang Y, Tyznik AJ, Self SG, Liggitt D, Rudensky AY. Recognition of the peripheral self by naturally arising CD25+ CD4+ T cell receptors. Immunity 2004; 21: 267–277.
15. Takahashi T, Kuniyasu Y, Toda M, Sakaguchi N, Itoh M, Iwata M et al. Immunologic self-tolerance maintained by CD25+CD4+ naturally anergic and suppressive T cells: Induction of autoimmune disease by breaking their anergic/suppressive state. Int Immunol 1998; 10: 1969–1980.
16. Nishimura E, Sakihama T, Setoguchi R, Tanaka K, Sakaguchi S. Induction of antigen-specific immunologic tolerance by *in vivo* and *in vitro* antigen-specific expansion of naturally arising Foxp3+CD25+CD4+ regulatory T cells. Int Immunol 2004; 16: 1189–1201.
17. Graca L, Thompson S, Lin CY, Adams E, Cobbold SP, Waldmann H. Both CD4(+)CD25(+) and CD4(+)CD25(−) regulatory cells mediate dominant transplantation tolerance. J Immunol 2002; 168: 5558–5565.
18. Hunig T. Manipulation of regulatory T-cell number and function with CD28-specific monoclonal antibodies. Adv Immunol 2007; 95: 111–148.
19. Siegmund K, Feuerer M, Siewert C et al. Migration matters: Regulatory T-cell compartmentalization determines suppressive activity *in vivo*. Blood 2005; 106: 3097–3104.
20. Haspot F, Séveno C, Dugast AS et al. Anti-CD28 antibody-induced kidney allograft tolerance related to tryptophan degradation and TCR class II B7 regulatory cells. Am J Transplant 2005; 5: 2339–2348.
21. Ford ML, Koehn BH, Wagener ME et al. Antigen-specific precursor frequency impacts T cell proliferation, differentiation, and requirement for costimulation. J Exp Med 2007; 204: 299–309.
22. Klein L, Khazaie K, von Boehmer H. *In vivo* dynamics of antigen-specific regulatory T cells not predicted from behavior *in vitro*. Proc Natl Acad Sci U S A 2003; 100: 8886–8891.
23. Walker LS, Chodos A, Eggena M, Dooms H, Abbas AK. Antigen-dependent proliferation of CD4+ CD25+ regulatory T cells *in vivo*. J Exp Med 2003; 198: 249–258.
24. Suntharalingam G, Perry MR, Ward S et al. Cytokine storm in a phase 1 trial of the anti-CD28 monoclonal antibody TGN1412. N Engl J Med 2006; 355: 1018–1028.
25. Stebbings R, Findlay L, Edwards C et al. "Cytokine storm" in the phase I trial of monoclonal antibody TGN1412: Better understanding the causes to improve preclinical testing of immunotherapeutics. J Immunol 2007; 179: 3325–3331.
26. Tang Q, Henriksen KJ, Bi M et al. *In vitro*-expanded antigen-specific regulatory T cells suppress autoimmune diabetes. J Exp Med 2004; 199: 1455–1465.
27. Tarbell KV, Yamazaki S, Olson K, Toy P, Steinman RM. CD25+ CD4+ T cells, expanded with dendritic cells presenting a single autoantigenic peptide, suppress autoimmune diabetes. J Exp Med 2004; 199: 1467–1477.
28. Beyersdorf N, Hanke T, Kerkau T, Hunig T. Superagonistic anti-CD28 antibodies: potent activators of regulatory T cells for the therapy of autoimmune diseases. Ann Rheum Dis 2005; 64(Suppl 4): iv91–iv95.

American Journal of Medical Genetics Part A 146A:2145–2151 (2008)

Clinical Report

The *CASK* Gene Harbored in a Deletion Detected by Array-CGH as a Potential Candidate for a Gene Causative of X-linked Dominant Mental Retardation

Shin Hayashi,[1,2,3] Seiji Mizuno,[4] Ohsuke Migita,[5] Torayuki Okuyama,[5] Yoshio Makita,[6] Akira Hata,[7] Issei Imoto,[1,2,3,8] and Johji Inazawa[1,2,3,8]*

[1]Department of Molecular Cytogenetics, Medical Research Institute and School of Biomedical Science, Tokyo Medical and Dental University, Tokyo, Japan
[2]21st Century Center of Excellence Program for Molecular Destruction and Reconstitution of Tooth and Bone, Tokyo Medical and Dental University, Tokyo, Japan
[3]Core Research for Evolutional Science and Technology (CREST) of Japan Science and Technology Corporation (JST), Saitama, Japan
[4]Department of Pediatrics, Central Hospital, Aichi Human Service Center, Kasugai, Japan
[5]Department of Clinical Genetics and Molecular Medicine, National Center for Child Health and Development, Tokyo, Japan
[6]Education Center, Asahikawa Medical College, Asahikawa, Japan
[7]Department of Public Health, Chiba University Graduate School of Medicine, Chiba, Japan
[8]Hard Tissue Genome research Center, Tokyo Medical and Dental University, Tokyo, Japan

Received 22 February 2008; Accepted 9 May 2008

Here we report on a 5-year-old Japanese girl with developmental delay and microcephaly. Although she had a normal karyotype, a bacterial artificial chromosome-based array-comparative genome hybridization analysis detected a de novo 4.0-Mb heterozygous deletion at Xp11.3–p11.4 harboring nine genes. By comparison with a healthy carrier mother of a boy with atypical Norrie disease having a smaller deletion in the same region, we excluded four genes as candidates whose haploinsufficiency would be causative for developmental delay. Among the other five genes, *CASK* seems to be the most likely candidate for a causative gene, because it is strongly expressed in fetal brain and plays important roles in neural development and synaptic function. We confirmed that the expression of CASK mRNA was decreased in the patient compared with healthy controls and the patient's X-chromosomal inactivation was not skewed. These results suggested that the genetic deletion of *CASK* results in haploinsufficiency, which might be causative for the patient's developmental delay or mental retardation.
© 2008 Wiley-Liss, Inc.

Key words: array-CGH; CASK; X-linked mental retardation; microcephaly; X-chromosome inactivation; del(X)(p11.3p11.4); Norrie disease

How to cite this article: Hayashi S, Mizuno S, Migita O, Okuyama T, Makita Y, Hata A, Imoto I, Inazawa J. 2008. The *CASK* gene harbored in a deletion detected by array-CGH as a potential candidate for a gene causative of X-linked dominant mental retardation. Am J Med Genet Part A 146A:2145–2151.

INTRODUCTION

Array-comparative genome hybridization (array-CGH) is useful for the detection of submicroscopic chromosome copy-number aberrations. We have analyzed patients with multiple congenital anomalies and mental retardation (MCA/MR) using custom bacterial artificial chromosome (BAC) array-CGH in cooperation with more than 20 medical institutions. In the primary screening, we used a "MCG Genome Disorder (GD) Array" containing 561 BAC clones (version 1.0) or 550 BAC clones (version 2.0) covering loci associated with known genomic

This article contains supplementary material, which may be viewed at the American Journal of Medical Genetics website at http://www.interscience.wiley.com/jpages/1552-4825/suppmat/index.html.

Grant sponsor: Ministry of Education, Culture, Sports, Science, and Technology, Japan; Grant sponsor: Core Research for Evolutional Science and Technology of the Japan Science and Technology Corporation; Grant sponsor: New Energy and Industrial Technology Development Organization.

*Correspondence to: Johji Inazawa, M.D., Ph.D., Department of Molecular Cytogenetics, Medical Research Institute, Tokyo Medical and Dental University, 1-5-45 Yushima Bunkyo-ku, Tokyo 113-8510, Japan. E-mail: johinaz.cgen@mri.tmd.ac.jp

DOI 10.1002/ajmg.a.32433

disorders and subtelomeric regions of all chromosomes, and in the secondary screening we used a "MCG Whole Genome (WG) Array-4500" which harbors 4523 BACs throughout the human genome [Inazawa et al., 2004]. Once we detected copy-number aberrations, which seem to correlate with specific disorders, we further analyzed other family members including parents to determine whether such alterations are de novo. In those cases, we also performed additional analyses, for example, array-CGH with higher density, fluorescence in situ hybridization (FISH), quantitative polymerase chain reaction (PCR) for genomic DNA or mRNA, and sequencing, to ascertain the correlation between copy-number aberrations/specific genes within altered regions and the pathogenesis of disorders [Hayashi et al., 2005, 2007].

Here, we report on a Japanese girl with developmental delay and microcephaly, whose 4.0-Mb heterozygous deletion at Xp11.3–p11.4 containing several genes was detected by array-CGH. We compared this deletion with a smaller deletion in the same region detected in a healthy carrier of atypical Norrie disease, and selected calcium/calmodulin-dependent serine protein kinase (*CASK*) as a candidate causative gene for developmetal delay or mental retardatation (MR). Our study, together with previous reports [Stevenson et al., 2000; Olsen et al., 2005; Hsueh, 2006; Froyen et al., 2007], suggests *CASK* is a potential candidate for X-linked dominant MR.

Clinical Reports

Patient 1

The subject was an almost 5-year-old Japanese girl (Fig. 1). She was born to nonconsanguineous healthy parents by normal spontaneous vaginal delivery at 39$$$$ weeks. At birth, her weight was 2,084 g (−2.7 SD), height was 42 cm (−3.9 SD), and occipitofrontal head circumference (OFC) was 28.8 cm (−3.1 SD). Her psychomotor development was delayed. She raised her head at age 6 months, sat at 3 years and stood with support at 4 years. Her developmental quotient (DQ) was 9 at 2 years old (in Kinder Infant Development Scale, which is a widely used developmental test In Japan).

FIG. 1. Facial features of Patient 1. Except for the microcephaly and strabismus, no prominent dysmorphic features were observed. [Color figure can be viewed in the online issue, which is available at www.interscience.wiley.com.]

At examination, her weight was 8.4 kg (−3.1 SD), height was 84 cm (−3.8 SD), and OFC was 39.5 cm (−6.0 SD). She had dysmorphic features including hirsutism, low hairline, arching of eyebrows with sparse lateral third, earlobe sinuses and micrognathia. However she had no structural ocular aberration. She had a squint with nystagmus and myopia. Her hands showed proximally placed thumbs, apparent brachydactyly and clinodactyly of the fifth fingers. She had no expressive speech. Magnetic resonance imaging (MRI) of her brain showed cerebellar atrophy. Atrophy was also observed at the mesencephalon and pons, although the cerebral cortex was not atrophic. A conventional peripheral blood karyotype of about 400–550 bands was 46,XX.

Patient 2

The subject was a 17-month-old Japanese boy diagnosed as having Norrie disease (ND, OMIM #310600) with psychomotor developmental retardation. At the time of examination he could not sit and spoke no words. A peripheral blood karyotype at the 400–550 band-level was 46,XY. Although a mutational analysis of the known causative gene, *NDP*, using genomic DNA was performed, PCR using primers spanning the gene yielded no products, indicating that he was nullizygous for the *NDP*.

MATERIALS AND METHODS

The research protocol was approved by the local ethics committees (Medical Research Institute, Tokyo Medical and Dental University, Japan; Aichi Human Service Center, Japan; and National Center for Child Health and Development, Japan). A lymphoblastoid cell line (LCL) was established as described previously [Saito-Ohara et al., 2002].

Among recently constructed in-house BAC-based arrays [Inazawa et al., 2004], we employed the "MCG WG Array-4500," and a "MCG X-tiling Array," which contains 1001 BAC/PACs throughout the X-chromosome other than peudoautosomal regions, for the array-CGH analysis. Hybridization was performed as described elsewhere [Hayashi et al., 2005, 2007]. Acquired images of hybridized slides were analyzed with GenePix Pro 6.0 imaging software (Axon Instruments, Foster City, CA). Fluorescence ratios were normalized so that the mean of the middle third of $\log_2$ ratios across the array was zero. The

thresholds for copy-number gain and loss were set at $\log_2$ ratios of 0.35 and −0.35, respectively.

Metaphase chromosomes were prepared from normal male lymphocytes and from the patients and patients' parents LCL by standard methods. The FISH was performed as described [Hayashi et al., 2005] using BACs around the regions of interest.

The pattern of X-chromosome inactivation was evaluated in metaphase chromosomes from LCL using the BrdU-labeling technique in late S-phase [Inazawa et al., 1993]. Those chromosomes were used for FISH to show the affected chromosome X as described elsewhere [Honda et al., 2007].

To investigate the expression of *CASK*, quantitative real-time RT-PCR experiments were performed with an ABI Prism 7900 sequence-detection system (Applied Biosystems, Foster City, CA) using SYBR Green PCR Master Mix (Applied Biosystems) according to the manufacturer's instructions. Two primer sets were designed between exon 10 (CTCCGAAGACCCTACCTCCT) and exon 13 (CACAAAGTCTTCACCACAAA) of *CASK*, respectively. Each assay was performed in triplicate. cDNA was synthesized from total RNA extracted from LCL of the patient, as well as four healthy males and four females as controls. Mutations within the coding sequence of *CASK* were analyzed by direct sequencing of genomic DNA extracted from LCL of the patient.

RESULTS

For Patient 1, we performed an array-CGH analysis using the "MCG WG Array-4500." Decreases ($\log_2$ ratio <-0.35) in the ratio of 11 BAC clones at Xp11.3p11.4 were detected (Fig. 2A), consistent with a heterozygous deletion. To determine the size of the deleted region, we performed a MCG X-tiling Array' analysis. This showed a deleted region of about 4.0-Mb spanning at Xp11.3p11.4 (Fig. 2B). The proximal boundary was between RP11-245M24 and RP11-467A17, whereas the distal boundary was probably included in clone RP11-1069J5 showing a slight decrease in the ratio. In concordance with ISCN 2005 [Shaffer and Tommerup, 2005], this result was described as follows; arr cgh Xp11.3p11.4(RP11-1069J5 → RP11-245M24)x1.

In Patient 2, a deletion in the region containing *NDP*, which is located at Xp11.3, was suspected because of the atypical phenotype of Norrie disease and no products in genomic PCR for this gene. A "MCG X-tiling Array" showed a ~650-kb complete loss ($\log_2$ ratio <-0.35) including the *NDP* gene at Xp11.3 (Fig. 2C); arr cgh Xp11.3(RP11-384A17 → RP11-110B2)x0. Array-CGH analysis detected a heterozygous deletion of the same region in his mother (Fig. 2D). The result was described as follows; arr cgh Xp11.3(RP11-384A17 → RP11-110B2)x1.

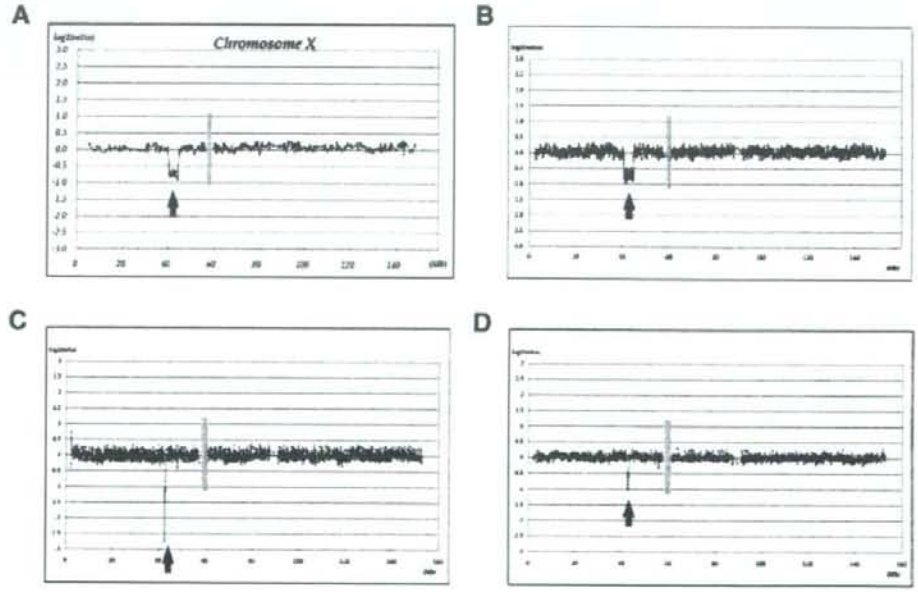

FIG. 2. Representative results of the array-CGH analyses. Clones are ordered according to the UCSC mapping position (http://genome.ucsc.edu/; Freeze March, 2006). Each spot represents the test/reference value after normalization and $\log_2$ transformation in each BAC clone. The gray vertical bar indicates a centromere. **A**: Profile of chromosome X in the MCG WG Array-4500 analysis for Patient 1. A deletion at Xp11.3p11.4 was detected (arrow). **B**: Result of the X-tiling array analysis for Patient 1. An approximately 4.0-Mb deletion at Xp11.3p11.4 was detected based on the reduced ratios of 33 BAC clones (arrow). **C**: Result of the X-tiling array analysis for Patient 2. An approximately 650-kb deletion at Xp11.3 was detected based on the reduced ratios of five BAC clones (arrow). **D**: Result of the X-tiling array analysis for the mother of Patient 2. The same deletion as in Patient 2 was detected at Xp11.3 (arrow).

To confirm the deletion, we performed FISH. In Patient 1, the probe RP11-95C16 showed a single copy loss on one allele of chromosome X (Fig. 3A), though this loss was detected in neither of her parents (Fig. 3B), indicating that the deletion in Patient 1 was de novo. Biological parentage was confirmed (data not shown) [Ingvarsson et al., 2000]. In Patient 2, the signal of the probe RP11-244N8 at Xp11.3 was completely lost (Fig. 3C), whereas it was lost on only one of the X chromosomes of the mother (Fig. 3D). The BAC clones and genes in Xp11.3p11.4 are shown in Figure 3E.

We assessed the X-inactivation status by FISH using BrdU-labeled metaphases. In Patient 1, an allele harboring the deletion showed late-replication indicative of an inactivated X in 11 of 20 metaphases (see the online Supplementary Fig. S1 at http://www.interscience.wiley.com/jpages/1552-4825/suppmat/index.html). X-inactivation was also estimated in the mother of Patient 2 and an allele harboring the deletion showed late-replication indicative of an inactivated X in 8 of 20 metaphases (data not shown). We conclude that X-chromosomal inactivation was not skewed in either case.

In Patient 1, the deletion included at least nine known protein-coding genes (Fig. 3E). We speculated that haploinsufficiency of one or more of these nine genes might cause the phenotype of the patient. Among these genes, we selected *CASK* as a candidate gene for the reasons described below. We assessed the expression level of *CASK* using quantitative real-time RT-PCR. It revealed a significant reduction of *CASK* expression in Patient 1 compared with four healthy males and four healthy females including the mother of Patient 2, and the expression in the healthy controls revealed no difference between sexes (Fig. 4).The coding sequence of *CASK* demonstrated no mutation in Patient 1 (data not shown).

DISCUSSION

In this study, we investigated copy-number changes in patient with developmental delay and microcephaly using array-CGH, and compared them with those in a carrier of atypical Norrie disease to determine a candidate causative gene for MR in females. In Patient 1, array-CGH detected a de novo 4.0-Mb heterozygous deletion at Xp11.3p11.4 har-

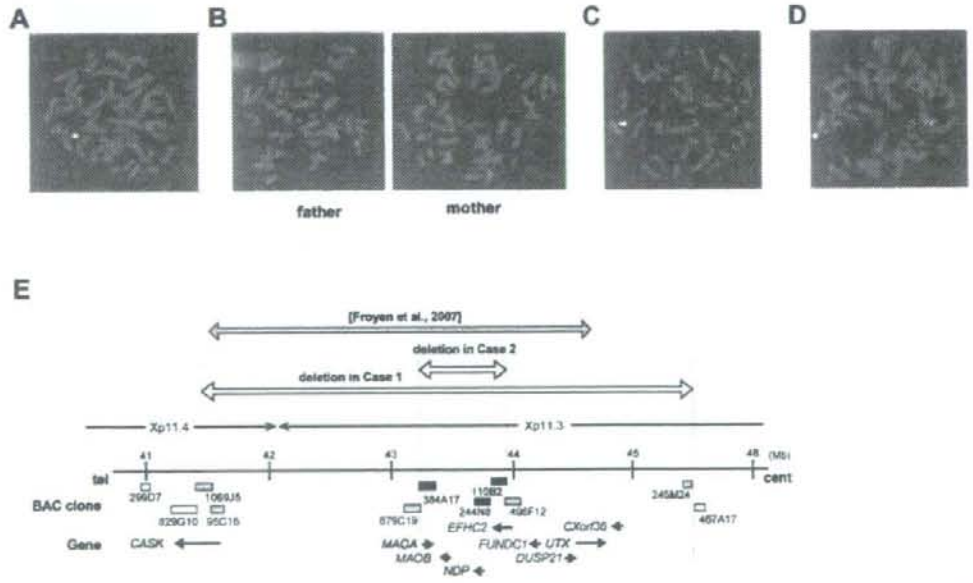

FIG. 3. Representative results of FISH analyses and schematic map of BAC clones and genes within the deleted region Xp11.3p11.4 in Patients 1 and 2. **A**: FISH for Patient 1 using a clone at Xp11.4 included in her deletion (RP11-95C16, red) and a reference clone at Xq28 (RP11-402H20, green). Yellow arrowhead denotes the deletion of RP11-95C16 on one allele. **B**: FISH for parents of Patient 1 using the same clone at Xp11.4 (RP11-95C16, red) and a reference clone at Xq22.2 (RP11-142J15, green). No deletion was observed in either parent. **C**: FISH for Patient 2 using a clone at Xp11.3 included in his deletion (RP11-244N8, red) and a reference clone at Xq22.3 (RP11-539A6, green). **D**: FISH for the mother of Patient 2 using RP11-244N8 (red) and a reference clone at Xq21.3 (RP11-111O14, green). RP11-244N8 was confirmed to hybridize correctly on chromosome X and yellow arrowhead denotes its deletion on one allele. **E**: Scheme of BAC clones and genes within the deleted region Xp11.3p11.4 in Patients 1 and 2. Thick horizontal bars indicate BAC clones used in the FISH analysis and spotted on the genome arrays. MCG WG Array-4500 and MCG X-tiling Array. Among clones on the arrays, only those around the boundary were drawn. Filled bars denote clones included in the deletions in Patient 1, Patient 2, and the mother of Patient 2; gray bars denote ones included in the deletion in only Patient 1; and open bars denote ones excluded from both deletions. Thin horizontal arrows indicate genes and their directions accord with the direction of the genes. Open double-headed arrows indicate the deletions of Patient 1 and Patient 2 respectively, and gray double-headed arrow indicates the deletion of the previously reported case [Froyen et al., 2007] for reference. *CASK* is on the boundary of the deletion in Patient 1. [Color figure can be viewed in the online issue, which is available at www.interscience.wiley.com.]

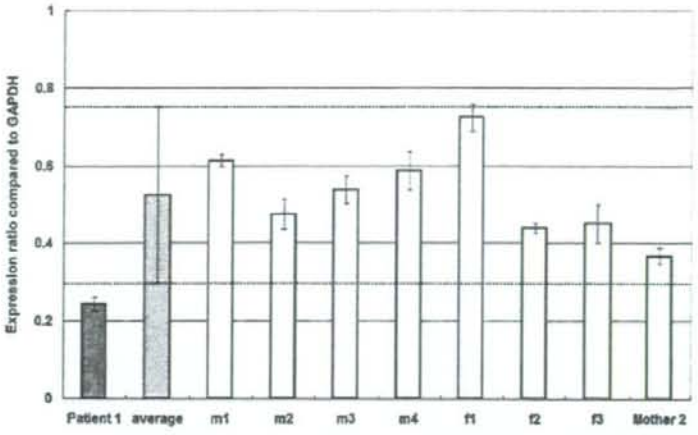

FIG. 4. Results of quantitative real-time PCR analysis for CASK expression. Primers were designed between exon 10 and exon 13 of *CASK*. "m1," "m2," "m3," and "m4" are four healthy males, and "f1," "f2," "f3," and "mother 2" are four healthy females including the mother of Patient 2 ("Mother 2" indicates). "Average" is the average of all eight healthy controls. Error bars indicate SD, and dashed horizontal lines indicate ± SD of the eight controls. Notably, *CASK* is normally expressed without sexual difference probably due to dosage compensation, whereas the expression of CASK was significantly decreased in Patient 1.

boring nine protein-coding genes (Fig. 3E). One or more of them were a potential causative gene(s) for the phenotype of patient 1. We narrowed the list of candidate genes by studying the phenotypically normal mother of a boy with atypical Norrie disease and a 650-kb deletion harboring the *NDP* gene at Xp11.3. This suggests that, consistent with previous reports [Collins et al., 1992; Rodriguez-Revenga et al., 2007], haploinsufficiency of genes within the heterozygously deleted region, such as *MAOA*, *MAOB*, *NDP*, and *EFHC2*, caused neither the MR nor the dysmorphologic phenotype. Therefore, these four genes can be excluded as candidates for the phenotype in Patient 1.

Among the other five genes, that is, *CASK*, *FUNDC*, *DUSP21*, *UTX*, and *CXorf36*, we focused on *CASK* because it was previously reported as a candidate MR gene [Froyen et al., 2007]. We excluded four other genes as candidates since each of their functions was reported to be associated with phosphorylation or demethylation, or unknown, respectively. *CASK* is highly expressed in the mammalian nervous system of both adults and fetuses [Stevenson et al., 2000], and to play several roles in neural development and synaptic function [Hsueh, 2006]. CASK enters the nucleus of neurons and interacts with Tbr-1 (T-brain-1), a T-box transcription factor, to activate the expression of genes involved in neural development, for example, reelin, which is essential for cerebrocortical development [Hsueh et al., 2000]. CASK also comprises a large protein complex with MALS (mammalian LIN-7) and Mint-1 (munc-18 interacting protein 1), which occurs on both sides of the synaptic junction and has a potential to link trans-synaptic adhesion [Olsen et al., 2005, 2006]. A potential function of this complex is controlling the release of transmitters at excitatory synapses via the recruitment of presynaptic vesicles. Genes encoding components of the complex are highly conserved and their mutations cause presynaptic defects [Olsen et al., 2005] or a reduction of axonal branching [Kaufmann et al., 2002], suggesting that the complex is crucial for proper functioning, although whether CASK has essential roles in synaptic function remains unclear. The knockout of *CASK* in mice was a prenatal lethal [Wilson et al., 1993; Laverty and Wilson, 1998], making the analysis of the role of CASK complicated. Cultured neurons lacking CASK were demonstrated to display overall normal electrical properties and form ultrastructurally normal synapses, but the spontaneous release of neurotransmitters was altered: glutamatergic synaptic release events are increased and GABAergic release events are decreased. Additionally, *CASK* mutant mice displayed cranial dysmorphology in both sexes and cleft palate only in males [Wilson et al., 1993]. Conditional knockout mice, in which CASK expression was decreased, were viable but significantly smaller than littermate controls [Atasoy et al., 2007]. These reports are consistent with the hypothesis that haploinsufficiency of *CASK* causes the CNS dysfunction in Patient 1. Since *CASK* was reported to be a gene not escaping an X-inactivation [Carrel and Willard, 2005] and X-inactivation was not skewed in Patient 1 (see the online Supplementary Fig. S1 at http://www.interscience.wiley.com/jpages/1552-4825/suppmat/index.html), the heterozygous deletion of this gene may result in the disruption of

dosage compensation [Franco and Ballabio, 2006] and cause developmental delay. Although the patient described by Froyen et al. [2007] resembles Patient 1 reported here, she was reported to show a more severe phenotype, which may result from the complete inactivation of her intact X chromosome [Froyen et al., 2007].

To date, over 60 X-linked mental retardation genes have been identified [Ropers and Hamel, 2005; Ropers, 2006]. Many of them cause MR in males, but not in females, as long as X-chromosomal inactivation is not skewed. However some of them, for example, *MECP2*, *MID1*, and *LAMP2*, are implicated in X-linked dominant disorders, because their haploinsufficiency also causes a phenotype in females [Franco and Ballabio, 2006]. Males with a loss of function of such genes would die, for example, *MECP2* [Villard, 2007], or have more severe phenotypes than females, for example, *MID1* [So et al., 2005]. We suggest that a male with a deletion of *CASK* would be lethal in a fetal period, and that CASK loss of function causes X-linked dominant inheritance of cognitive impairment.

MOLECULAR DATABASES

We used the NCBI mRNA reference sequences track in the UCSC browser (http://genome.ucsc.edu/), March 2006 assembly to assess gene content of this region.

ACKNOWLEDGMENTS

We thank Ayako Takahashi and Rumi Mori for technical assistance. This work was supported by grants-in-aid for Scientific Research on Priority Areas and 21st Century Center of Excellence Program for Molecular Destruction and Reconstitution of Tooth and Bone from the Ministry of Education, Culture, Sports, Science, and Technology, Japan; a grant from Core Research for Evolutional Science and Technology of the Japan Science and Technology Corporation; and a grant from the New Energy and Industrial Technology Development Organization.

REFERENCES

Atasoy D, Schoch S, Ho A, Nadasy KA, Liu X, Zhang W, Mukherjee K, Nosyreva ED, Fernandez-Chacon R, Missler M, Kavalali ET, Südhof TC. 2007. Deletion of CASK in mice is lethal and impairs synaptic function. Proc Natl Acad Sci USA 104:2525–2530.

Carrel L, Willard HF. 2005. X-inactivation profile reveals extensive variability in X-linked gene expression in females. Nature 434:400–404.

Collins FA, Murphy DL, Reiss AL, Sims KB, Lewis JG, Freund L, Karoum F, Zhu D, Maumenee IH, Antonarakis SE. 1992. Clinical, biochemical, and neuropsychiatric evaluation of a patient with a contiguous gene syndrome due to a microdeletion Xp11.3 including the Norrie disease locus and monoamine oxidase (MAOA and MAOB) genes. Am J Med Genet 42:127–134.

Franco B, Ballabio A. 2006. X-inactivation and human disease: X-linked dominant male-lethal disorders. Curr Opin Genet Dev 16:254–259.

Froyen G, Van Esch H, Bauters M, Hollanders K, Frints SG, Vermeesch JR, Devriendt K, Fryns JP, Marynen P. 2007. Detection of genomic copy number changes in patients with idiopathic mental retardation by high-resolution X-array-CGH: Important role for increased gene dosage of XLMR genes. Hum Mut 28:1034–1042.

Hayashi S, Kurosawa K, Imoto I, Mizutani S, Inazawa J. 2005. Detection of cryptic chromosome aberrations in a patient with a balanced t(1;9)(p34.2;p24) by array-based comparative genomic hybridization. Am J Med Genet Part A 139A:32–36.

Hayashi S, Honda S, Minaguchi M, Makita Y, Okamoto N, Kosaki R, Okuyama T, Imoto I, Mizutani S, Inazawa J. 2007. Construction of a high-density and high-resolution human chromosome X array for comparative genomic hybridization analysis. J Hum Genet 52:397–405.

Honda S, Hayashi S, Kato M, Niida Y, Hayasaka K, Okuyama T, Imoto I, Mizutani S, Inazawa J. 2007. Clinical and molecular cytogenetic characterization of two patients with non-mutational aberrations of the FMR2 gene. Am J Med Genet Part A 143A:687–693.

Hsueh YP. 2006. The role of the MAGUK protein CASK in neural development and synaptic function. Curr Med Chem 13:1915–1927.

Hsueh YP, Wang TF, Yang FC, Sheng M. 2000. Nuclear translocation and transcription regulation by the membrane-associated guanylate kinase CASK/LIN-2. Nature 404:298–302.

Inazawa J, Azuma T, Ariyama T, Abe T. 1993. A simple G-banding technique adaptable for fluorescent *in situ* hybridization (FISH) and physical ordering of human renin (REN) and cathepsin E (CTSE) genes by multi-color FISH. Acta Histochem Cytochem 26:319–324.

Inazawa J, Inoue J, Imoto I. 2004. Comparative genomic hybridization (CGH)-arrays pave the way for identification of novel cancer-related genes. Cancer Sci 95:559–563.

Ingvarsson S, Finnsdottir V, Sigurdsson A, Geirsson G. 2000. Population studies and validation of paternity determinations by six microsatellite loci. J Forensic Sci 45:692–695.

Kaufmann N, DeProto J, Ranjan R, Wan H, van Vactor D. 2002. Drosophila liprin-alpha and the receptor phosphatase Dlar control synapse morphogenesis. Neuron 34:27–38.

Laverty HG, Wilson JB. 1998. Murine CASK is disrupted in a sex-linked cleft palate mouse mutant. Genomics 53:29–41.

Olsen O, Moore KA, Fukata M, Kazuta T, Trinidad JC, Kauer FW, Streuli M, Misawa H, Burlingame AL, Nicoll RA, Bredt DS. 2005. Neurotransmitter release regulated by a MALS-liprin-alpha presynaptic complex. J Cell Biol 170:1127–1134.

Olsen O, Moore KA, Nicoll RA, Bredt DS. 2006. Synaptic transmission regulated by a presynaptic MALS/Liprin-alpha protein complex. Curr Opin Cell Biol 18:223–227.

Rodriguez-Revenga L, Madrigal I, Alkhalidi LS, Armengol L, González E, Badenas C, Estivill X, Milà M. 2007. Contiguous deletion of the NDP, MAOA, MAOB, and EFHC2 genes in a patient with Norrie disease, severe psychomotor retardation and myoclonic epilepsy. Am J Med Genet Part A 143A:916–920.

Ropers HH. 2006. X-linked mental retardation: Many genes for a complex disorder. Curr Opin Genet 16:260–269.

Ropers HH, Hamel BC. 2005. X-linked mental retardation. Nat Rev Genet 6:46–57.

Saito-Ohara F, Fukuda Y, Ito M, Agarwala KL, Hayashi M, Matsuo M, Imoto I, Yamakawa K, Nakamura Y, Inazawa J. 2002. The Xq22 inversion breakpoint interrupted a novel Ras-like GTPase gene in a patient with Duchenne muscular dystrophy and profound mental retardation. Am J Hum Genet 71:637–645.

Shaffer LG, Tommerup N. 2005. An international system for human cytogenetic nomenclature (2005). Basel: Karger. p 118–120.

So J, Suckow V, Kijas Z, Kalscheuer V, Moser B, Winter J, Baars M, Firth H, Lunt P, Hamel B, Meinecke P, Moraine C, Odent S, Schinzel A, van der Smagt JJ, Devriendt K, Albrecht B, Gillessen-Kaesbach G, van der Burgt I, Petrij F, Faivre L, McGaughran J, McKenzie F, Opitz JM, Cox T, Schweiger S. 2005. Mild phenotypes in a series of patients with Opitz GBBB syndrome with MID1 mutations. Am J Med Genet Part A 132A:1–7.

Stevenson D, Laverty HG, Wenwieser S, Douglas M, Wilson JB. 2000. Mapping and expression analysis of the human CASK gene. Mamm Genome 11:934–937.

Villard L. 2007. MECP2 mutations in males. J Med Genet 44:417–423.

Wilson JB, Ferguson MW, Jenkins NA, Lock LF, Copeland NG, Levine AJ. 1993. Transgenic mouse model of X-linked cleft palate. Cell Growth Differ 4:67–76.

J Hum Genet (2008) 53:467–474
DOI 10.1007/s10038-008-0272-4

ORIGINAL ARTICLE

Structural study on mutant α-L-iduronidases: insight into mucopolysaccharidosis type I

Kanako Sugawara · Seiji Saito · Kazuki Ohno · Torayuki Okuyama · Hitoshi Sakuraba

Received: 16 January 2008 / Accepted: 15 February 2008 / Published online: 14 March 2008

Abstract To elucidate the basis of mucopolysaccharidosis type I (MPS I), we constructed structural models of mutant α-L-iduronidases (IDUAs) resulting from 33 amino acid substitutions that lead to MPS I (17 severe, eight intermediate, and eight attenuated). Then, we examined the structural changes in the enzyme protein by calculating the number of atoms affected and determined the root-mean-square distance (RMSD) and the solvent-accessible surface area (ASA). In the severe MPS I group, the number of atoms influenced by a mutation and the average RMSD value were larger than those in the attenuated group, and the residues associated with the mutations identified in the severe group tended to be less solvent accessible than those in the attenuated group. The clinically intermediate phenotype group exhibited intermediate values for the numbers of atoms affected, RMSD, and ASA between those in the severe group and those in the attenuated group. The results indicated that large structural changes had occurred in the core region in the severe MPS I group and small ones on the molecular surface in the attenuated MPS I group. Color imaging revealed the distributions and degrees of the structural changes caused by representative mutations for MPS I. Thus, structural analysis is useful for elucidating the basis of MPS I. As there was a difference in IDUA structural change between the severe MPS I group and the attenuated one, except for a couple of mutations, structural analysis can help predict the clinical outcome of the disease.

Keywords Mucopolysaccharidosis type I · Hurler syndrome · Scheie syndrome · Hurler/Scheie syndrome · α-L-Iduronidase · Protein structure

Disclaimers: None

Electronic supplementary material The online version of this article (doi:10.1007/s10038-008-0272-4) contains supplementary material, which is available to authorized users.

K. Sugawara · H. Sakuraba (✉)
Department of Analytical Biochemistry,
Meiji Pharmaceutical University, 2-522-1 Noshio,
Kiyose, Tokyo 204-8588, Japan
e-mail: sakuraba@my-pharm.ac.jp

S. Saito
Graduate School of Agricultural and Life Science,
The University of Tokyo, Tokyo, Japan

K. Ohno
Center for Biological Resources and Informatics,
Tokyo Institute of Technology, Yokohama, Japan

T. Okuyama
Department of Clinical Laboratory Medicine,
National Center for Child Health and Development,
Tokyo, Japan

Present Address:
K. Ohno
Drug Discovery Research, Astellas Pharm Inc,
Tsukuba, Japan

Introduction

Alpha-L-iduronidase (IDUA; E.C.3.2.1.76) is an acid glycosidase involved in the degradation of glycosaminoglycans (GAGs) heparan sulfate and dermatan sulfate. Defects in the *IDUA* gene result in a human metabolic disease, mucopolysaccharidosis type I (MPS I; McKusick 25280), causing impaired degradation of GAGs and their systemic deposition (Neufeld and Muenzer 2001). The disease exhibits a wide clinical spectrum. The most severe

phenotype with early onset (Hurler syndrome, MPS IH) involves mental retardation, skeletal deformities, stiff joints, hepatosplenomegaly, corneal clouding, and a shortened life expectancy. The attenuated phenotype with late onset (Scheie syndrome, MPS IS) involves mild skeletal deformities, stiff joints, corneal clouding, and a long life span without mental retardation. Furthermore, there is a clinically intermediate phenotype (Hurler/Scheie syndrome, MPS IH/S). As there are marked differences between the severe and attenuated phenotypes, they must be due to different recessive mutations of the *IDUA* gene and different expressed products, but the details have not yet been determined.

The *IDUA* gene spans 19 kb, includes 14 exons (Scott et al. 1992), and is localized to 4p16.3 (Scott et al. 1990). It encodes a precursor IDUA composed of a 653-amino acid polypeptide, the enzyme being glycosylated and then processed to the mature form (Tylor et al. 1991; Brooks 1993). As to the active site of IDUA, Brooks et al. (2001) predicted the putative acid/base catalyst and nucleophile residues to be E182 and E299, respectively. Then, they expressed site-directed mutants E182A and E299A in Chinese hamster ovary (CHO)-K1 cells and showed that the mutant proteins were catalytically inactive. These results suggest that these residues are important for the catalytic mechanism of IDUA.

So far, many gene mutations causing MPS I have been reported (Neufeld and Muenzer 2001; Yamagishi et al. 1996). Among them, gross alterations of the *IDUA* gene have been generally found in patients with the severe form, but missense mutations comprising the majority of mutations in MPS I have been identified in both the severe and milder forms, i.e., the intermediate and attenuated ones. As a recombinant human IDUA (laronidase; Genzyme, MA, USA) has been developed and introduced to enzyme replacement therapy for MPS I (Brooks 2002), prediction of the clinical outcome of the disease is becoming more and more important for determining the proper therapeutic schedule in the early stage of MPS I. To elucidate the basis of MPS I and to predict the clinical outcome of this disease, structural information on a defective IDUA is very important. However, only few reports on this issue have been published. Rempel et al. (2005) constructed a homology model for IDUA based on the crystal structure of the β-xylosidase from *Thermoanaerobacterium saccharolyticum*, predicted the location of residues associated with MPS I in the IDUA structure, and analyzed the structural differences in amino acid chains.

In this study, we built structural models of mutant IDUA proteins resulting from amino acid substitutions responsible for severe, intermediate, and attenuated MPS I. We then examined their structural changes by calculating the number of atoms influenced by the amino acid substitutions and by determining the root-mean-square distance (RMSD) and the solvent-accessible surface area (ASA). Furthermore, we examined the distributions and degrees of three-dimensional structural changes caused by representative mutations by means of color imaging.

Materials and methods

Amino acid substitutions causing severe, intermediate, and attenuated MPS I

So far, more than 40 missense mutations associated with MPS I have been reported. We here analyzed 33 amino acid replacements for which the phenotypes have been clearly described (17 severe, eight intermediate, and eight attenuated). The amino acid substitutions, their phenotypes, and references are summarized in Table 1.

Structural modeling of mutant IDUA proteins, and calculation of the number of atoms influenced by amino acid substitutions responsible for MPS I

Structural models of mutant IDUAs were built using molecular modeling software TINKER, developed by Ponder et al. (Department of Biochemistry and Molecular Biophysics, Washington University) (Kundrot et al. 1991; Dudek and Ponder 1995; Kong and Ponder 1997; Pappu et al. 1998; Ren and Ponder 2003). As a template, the homology model of human IDUA (PDB: 1Y24) (Rempel et al. 2005) was used, and energy minimization was performed. The root-mean-square graduate value was set at 0.05 kcal/mol Å. Then, each mutant model was superimposed on the wild-type structure based on the Cα atoms by the least-square-mean fitting method (Kabsch 1976, 1978; Sakuraba et al. 2000, 2004; Matsuzawa et al. 2003, 2005). We defined that the structure was influenced by an amino acid substitution when the position of an atom in a mutant differed from that in the wild type by more than the cutoff distance (0.15 Å) based on the total RMSD, as described previously (Matsuzawa et al. 2005). We calculated the numbers of influenced atoms in the main chain and the side chain.

Determination of RMSD values of all atoms in mutant IDUAs

To compare the influences on conformational changes in IDUA by amino acid substitutions, the RMSD values of all atoms in mutant IDUAs were calculated according to the standard method (Weiner et al. 1984), and the average RMSDs for the severe, intermediate, and attenuated MPS I groups were determined.

Table 1 Mucopolysaccharidosis type I (MPS I) mutations, structural changes in α-L-iduronidases (IDUA), and phenotypes

Mutation	Numbers of affected atoms		RMSD (Å)	ASA (Å^2)	Phenotype	Reference
	Main chain	Side chain				
G51D	142	190	0.155	0	Severe	Venturi et al. (2002)
A75T	0	0	0.002	40.7	Severe	Clarke et al. (1994)
A160D	76	80	0.067	6.1	Severe	Venturi et al. (2002)
E182K	227	277	0.139	17.3	Severe	Matte et al. (2003)
P183R	223	256	0.14	0.4	Severe	Venturi et al. (2002)
G208D	57	62	0.066	5.2	Severe	Matte et al. (2003)
G208V	103	88	0.091	5.2	Severe	Beesley et al. (2001)
L218P	35	48	0.059	9.5	Severe	Bunge et al. (1994a)
I270S	0	3	0.003	60.1	Severe	Laradi et al. (2005)
D315Y	91	90	0.124	17.3	Severe	Li et al. (2002)
A327P	3	4	0.019	0.3	Severe	Bunge et al. (1994a)
D349Y	84	119	0.095	3.2	Severe	Matte et al. (2003)
R363C	47	48	0.041	52.7	Severe	Yogalingam et al. (2004)
T366P	64	56	0.081	12.6	Severe	Scott et al. (1995)
T388R	68	74	0.056	14.3	Severe	Rempel et al. (2005)
R489P	95	113	0.093	27.7	Severe	Bunge et al. (1994b)
P496R	533	511	0.245	0	Severe	Beesley et al. (2001)
A79V	11	6	0.025	53.7	Intermediate	Yogalingam et al. (2004)
H82P	125	159	0.127	47.2	Intermediate	Clarke et al. (1994)
E178K	155	234	0.111	3.6	Intermediate	Venturi et al. (2002)
S260F	0	2	0.011	64.2	Intermediate	Matte et al. (2003)
L346R	66	91	0.055	14.8	Intermediate	Teng et al. (2000)
T364M	0	0	0.002	39.2	Intermediate	Lee-Chen and Wang (1997)
L490P	28	24	0.056	111.4	Intermediate	Tieu et al. (1995)
P496L	135	121	0.115	0	Intermediate	Tieu et al. (1995)
R89Q	109	144	0.077	0.8	Attenuated	Scott et al. (1993)
C205Y	28	38	0.05	1.3	Attenuated	Beesley et al. (2001)
H240R	5	0	0.011	146.6	Attenuated	Beesley et al. (2001)
A319V	0	0	0.002	48.8	Attenuated	Beesley et al. (2001)
N350I	6	15	0.019	57.5	Attenuated	Matte et al. (2003)
Q380R	17	22	0.031	26.9	Attenuated	Beesley et al. (2001)
R383H	21	29	0.031	41.9	Attenuated	Clarke et al. (1994)
R492P	14	13	0.022	145.6	Attenuated	Tieu et al. (1995)

RMSD root-mean-squares distance, *ASA* solvent-accessible surface area

Determination of ASA of amino acid residues

The ASA of each amino acid residue in the wild-type IDUA was calculated using ACCESS (McDonald and Thornton 1994). As an input structure, the homology model of human IDUA was used. Then, the average ASA values of the residues for which a substitution had been identified in the severe, intermediate, and attenuated MPS I groups were determined.

Statistical analysis

Statistical analysis to determine the differences in the numbers of influenced atoms, the RMSD, and the ASA between the severe MPS I and attenuated groups, between the severe MPS I and milder ones (the intermediate and attenuated groups), between the severe MPS I and intermediate ones, and between the intermediate MPS I and attenuated ones was performed by means of the F test, and then Welch's t test, it being taken that there was a significant difference if $P < 0.05$.

Color imaging of the atoms influenced by representative amino acid substitutions causing MPS I

Color imaging of the influenced atoms in the three-dimensional structure of IDUA was performed for amino

acid substitutions including P496R (severe), H240R (attenuated), and E182K (severe). For these cases, clinical and biochemical investigations had been performed in detail (Brooks et al. 2001; Beesley et al. 2001; Matte et al. 2003). The analysis was based on the distances between the wild type and mutant to determine the influence of the amino acid substitutions geographically and semiquantitatively according to the method previously described (Matsuzawa et al. 2005).

Results

Numbers of atoms influenced by amino acid substitutions associated with MPS I

According to the structural model of human IDUA, the IDUA consists of two domains: a $(\beta/\alpha)_8$-barrel domain, and an antiparallel β-sheet domain (Rampel et al. 2005). To elucidate the basis of MPS I and to determine the relationship between the structural change caused by an amino acid substitution and the MPS I phenotype, we identified the locations of residues for amino acid substitutions and those of the putative acid/base catalyst (E182) and nucleophile (E299) in the structure of the wild-type IDUA (Fig. 1).

Then, we built structural models of the mutant IDUAs and calculated the numbers of atoms influenced by the amino acid substitution for each mutant model (Table 1). For the severe MPS I group, the averages for the influenced atoms in the main chain and the side chain were 109 and 119, respectively. In particular, regarding the former, 13 of the 17 severe cases (76%) had 40 atoms or more influenced (Fig. 2, left). On the other hand, the number of influenced atoms in the attenuated MPS I group was low. The averages of the influenced atoms in the main chain and the side chain were 27 and 33, respectively. In particular, regarding main-chain atoms, six of the seven attenuated cases (88%) had 39 atoms or less affected (Fig. 2, right). The F test indicated that the distributions exhibited unequal variance ($P < 0.05$) between the two groups, and thus Welch's t test was performed. The results revealed that there was a significant difference in the number of influenced atoms in both the main chain and the side chain ($P < 0.05$) between the severe and attenuated groups. As to the intermediate group, the averages of the influenced atoms in the main chain and the side chain were 65 and 80, respectively, indicating the values are intermediate between those of the severe and attenuated groups. The F test followed by Welch's t test revealed that there were significant differences ($P < 0.05$) in both the main chain and side chain between the severe and milder groups (the intermediate and attenuated groups). However, we could not statistically find any significant differences in the average numbers of atoms influenced between the severe and intermediate groups or between the intermediate and attenuated ones. These results suggest that structural changes caused by the amino acid substitutions responsible for severe MPS I are generally large, those for attenuated MPS I being small, and the structural changes tend to be correlated with the severity of the phenotype.

RMSD for MPS I mutations

The average RMSDs for the MPS I groups were determined and compared with each other to determine mutation

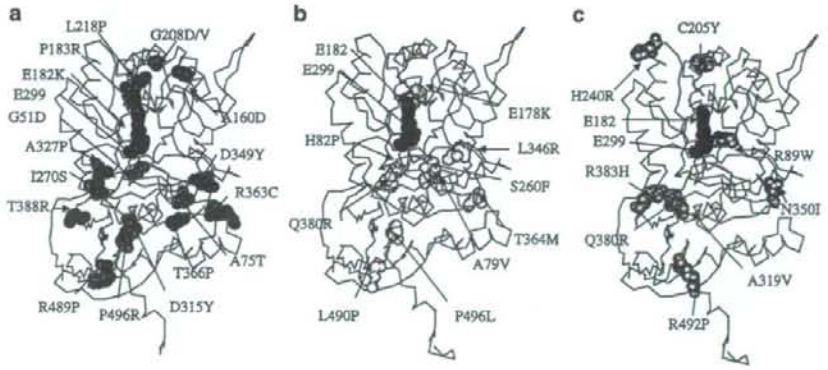

Fig. 1 Localization of missense mutations causing mucopolysaccharidosis type I (MPS I) and amino acid residues involved in the catalysis of the substrate in the three-dimensional structure of α-L-iduronidases (IDUA). The positions of amino acid substitutions are indicated as space-filling models. **a**, **b**, and **c** show the residues for the severe (*red*), intermediate (*yellow*), and attenuated (*orange*) MPS I cases, respectively. The putative acid/base catalyst (E182) and nucleophile (E299) residues in the active site are indicated as space-filling models (*blue*), except for E182 in **a**. In **a**, E182 was indicated as a space-filling model (*green*), as E182K had been identified in a patient with severe MPS I